Collective flow and two-pion correlations from a relativistic hydrodynamic model with early chemical freeze-out

Tetsufumi Hirano[1,*] and Keiichi Tsuda[2]
[1]*Physics Department, University of Tokyo, Tokyo 113-0033, Japan*
[2]*Department of Physics, Waseda University, Tokyo 169-8555, Japan*
(Received 8 August 2002; published 27 November 2002)

We investigate the effect of early chemical freeze-out on radial flow, elliptic flow, and Hanbury Brown–Twiss (HBT) radii by using a fully three-dimensional hydrodynamic model. When we take account of the early chemical freeze-out, the space-time evolution of temperature in the hadron phase is considerably different from the conventional model in which chemical equilibrium is always assumed. As a result, we find that radial and elliptic flows are suppressed and that the lifetime and the spatial size of the fluid are reduced. We analyze the p_t spectrum, the differential elliptic flow, and the HBT radii at the Relativistic Heavy-Ion Collider energy by using hydrodynamics with a chemically nonequilibrium equation of state.

DOI: 10.1103/PhysRevC.66.054905 PACS number(s): 25.75.Ld, 24.10.Nz

I. INTRODUCTION

One of the main topics in the physics of relativistic heavy-ion collisions is a detailed description of space-time evolution for the hot and dense nuclear matter by using a dynamical model such as kinetic transport models [1] or hydrodynamics [2]. Recent experimental data from Relativistic Heavy-Ion Collider (RHIC) suggest that we may see the significant effect of jet quenching in transverse momentum distribution for neutral pions [3] or azimuthal asymmetry for charged hadrons [4]. So hydrodynamic simulations of expanding hot and/or dense matter are indispensable in quantitatively estimating the effect of the medium on the jet quenching [5]. One of the authors (T.H.) has already built a fully three-dimensional hydrodynamic model which describes not only central but also noncentral collisions [6]. In contrary to other hydrodynamic models, e.g., (2+1) dimensional models with the Bjorken's scaling solution [7–9] or (3+1) dimensional models with cylindrical symmetry along the collision axis [10–13], full (3+1) dimensional hydrodynamic models [14–19] enable us to obtain the rapidity dependence of particle distribution, elliptic flow, and Hanbury Brown–Twiss (HBT) radii in *noncentral* collisions.

Statistical and hydrodynamics-motivated models give us the characteristic temperatures in relativistic heavy-ion collisions. These temperatures are very useful in understanding what happens in collisions. From fitting the model calculation of particle ratios for hadrons to the experimental data, the chemical freeze-out temperature $T^{\rm ch}$ is obtained at each collision energy [20–25]. On the other hand, we can obtain the thermal (kinetic) freeze-out temperature $T^{\rm th}$ from the slopes of a transverse momentum distribution by assuming the radial flow profile [22,26,27]. The temperatures obtained above are usually different from each other at the alternating gradient synchrotron, SPS, and probably RHIC energies: $T^{\rm ch}\sim 160-200$ MeV while $T^{\rm th}\sim 100-140$ MeV. The chemical freeze-out parameters $(T^{\rm ch},\mu_{\rm B}^{\rm ch})$ at various collision energies seem to be aligned on one line in the T-$\mu_{\rm B}$ plane. This line is sometimes called the ''chemical freeze-out line'' and can be parametrized by the average energy per particle $\langle E\rangle/\langle N\rangle\sim 1$ GeV [22]. Those analyses indicate that the system undergoes first the chemical freeze-out where the observed particle ratios are fixed and next the thermal freeze-out where the shape of the transverse momentum distribution is fixed [28]. Since the time scale of the hydrodynamic evolution is comparable with (or smaller than) that of the inelastic collisions between hadrons, the number changing processes are likely to be out of equilibrium. This is the reason why there are two sequential freeze-out processes in relativistic heavy-ion collisions. To give a more realistic description of the temporal and spatial behavior of the hot and dense matter, the above pictures should be included in the model. This makes us approach the comprehensive understanding of the deconfined matter, the quark gluon plasma (QGP).

In this paper, we incorporate the different freeze-out temperatures, $T^{\rm ch}$ and $T^{\rm th}$, into hydrodynamics and discuss how the early chemical freeze-out affects the space-time evolution of fluids and the particle spectra [29]. In the ordinary hydrodynamic calculations, one assumes both chemical and thermal equilibria and consequently $T^{\rm ch}=T^{\rm th}$ which is to be determined from comparison of the slopes of the transverse spectrum with the experimental data. If the system obeys the above picture of early chemical freeze-out, those ordinary hydrodynamic models can hardly reproduce the particle ratios due to the smallness of the chemical freeze-out temperature. As a result, the number of resonance particles at the thermal freeze-out becomes too small. The physics at the low transverse momentum is largely affected by resonance decays after thermal freeze-out. For example, the low p_t enhancement in the transverse momentum spectrum for pions can be explained by the contribution from resonance decays [30,31]. The slope of the p_t spectrum for pions directly emitted from the freeze-out hypersurface is almost constant. On the other hand, data for pions at low p_t show a steeper slope than those in the medium p_t region (~ 1 GeV/c). So one cannot reproduce the low p_t enhancement only from direct pions. Pions from ρ, ω, or Δ decays show a steeper p_t

*Electronic address: hirano@nt.phys.s.u-tokyo.ac.jp

spectrum than direct pions. We naturally explain the low p_t enhancement seen in the experimental data by resonance decays. Another example is the reduction of the second Fourier coefficient of the azimuthal distribution for pions at low p_t [32]. From the exact treatment of the decay kinematics, pions from resonance decays can pretend *out-of-plane* elliptic flow even when the hydrodynamic flow shows *in-plane* elliptic flow. This dilutes elliptic flow from direct pions. Therefore the early chemical freeze-out must be included in hydrodynamics in order to analyze not only the particle ratios but also the single-particle spectra and the azimuthal asymmetry.

This paper is organized as follows: We construct the equation of state for the hadron phase with and without chemical equilibria in Sec. II. We parametrize the initial condition for hydrodynamic simulations in the full three dimensional Bjorken coordinate in Sec. III. By using these equations of state and the initial condition, we perform hydrodynamic simulations in full three dimensional space at the RHIC energy and compare space-time evolutions with each other in Sec. IV. We analyze the particle spectra and the azimuthal asymmetry at the RHIC energy and discuss the effect of early chemical freeze-out on observables in Sec. V. We also analyze the two-pion correlation functions to see the effect on the hydrodynamic evolution in Sec. VI. A summary and discussions are given in Sec. VII.

II. EQUATIONS OF STATE

We assume the following picture of space-time evolution for hot and/or dense matter produced in relativistic heavy-ion collisions. First, the huge number of secondary partons are produced and both chemical and thermal equilibria among these partons are achieved in the early stage of collisions. The initial dominant longitudinal flow and the large pressure gradient perpendicular to the collision axis cause the system to expand and cool down. When the temperature of the system reaches the critical temperature T_c, the hadronization starts to occur. Just after the hadronization finishes, the chemical freeze-out happens at $T^{\rm ch}(\leqslant T_c)$. Below $T^{\rm ch}$, the ratios of the number of observed particles are fixed. Even after chemical freeze-out, the system keeps thermal equilibrium through elastic scattering. Finally, all hadrons are thermally frozen at $T^{\rm th}(<T^{\rm ch})$. If we neglect dissipation in the space-time evolution of nuclear matter, we can apply the hydrodynamic equations for the perfect fluid, $\partial_\mu T^{\mu\nu}=0$ and $\partial_\mu n_{\rm B}^\mu=0$, where $T^{\mu\nu}=(E+P)u^\mu u^\nu - P g^{\mu\nu}$ and $n_{\rm B}^\mu = n_{\rm B} u^\mu$ are energy momentum tensor and baryon density current, respectively. E, P, $n_{\rm B}$, and u^μ are energy density, pressure, baryon density, and four fluid velocity. With the help of thermodynamical identities and the baryon density conservation, the first equation is rewritten as $\partial_\mu s^\mu = 0$, where s^μ is the entropy current. These equations mean that a fluid element evolves along an adiabatic path ($n_{\rm B}/s = {\rm const}$) in the $T-\mu_{\rm B}$ plane. We assume this fact is approximately valid even below the chemical freeze-out line.

When N stable hadrons in the equation of state (EOS) undergo chemical freeze-out across the chemical freeze-out line, we can introduce chemical potentials μ_i associated with those hadrons. Then we may construct the EOS in the $(N+2)$ dimensional space (N for μ_i and 2 for T and $\mu_{\rm B}$). This causes a serious problem when we numerically simulate a hydrodynamic model with finite resources of memory. Since the chemical potential of each hadron depends on $T^{\rm ch}$, $\mu_{\rm B}^{\rm ch}$, T, and $\mu_{\rm B}$ during expansion along an adiabatic path, we can restrict ourselves to the EOS in a two-dimensional hypersurface $\mu_i = \mu_i(T,\mu_{\rm B})$ embedded in the $(N+2)$ dimensional space. Thus we need not prepare such a large dimensional table of the EOS anymore. When we obtain μ_i at a point $(T,\mu_{\rm B})$ below the chemical freeze-out line, we need the information at the chemical freeze-out point $(T^{\rm ch},\mu_{\rm B}^{\rm ch})$ somewhere on the chemical freeze-out line and have to go back to the point along an adiabatic path. Since the adiabatic path itself is obtained from the thermodynamical variables and $\mu_i(T,\mu_{\rm B})$, we have to solve the problem self-consistently. In this paper, we restrict our discussion to the zero baryonic chemical potential where the adiabatic path becomes a trivial one, $n_{\rm B}/s=0$. This is good approximation in Au + Au $\sqrt{s_{NN}}=130$ GeV collisions in which $\bar{p}/p \sim 0.6$ [33–36] or the resultant chemical freeze-out parameter $\mu_{\rm B}^{\rm ch} \sim 50$ MeV [24].

We construct three model EOS's to compare the space-time evolution of fluids. These models describe the first order phase transition between the QGP phase and the hadron phase at $T_c = 170$ MeV. We suppose the QGP phase is composed of massless u,d, and s quarks and gluons and that this is common to three models. The EOS for the QGP phase is $P=(E-4B)/3$, where B is a bag constant specified later. For the hadron phase, we choose three different model EOS's as follows.

A. Chemical equilibrium

The first model is an ordinary resonance gas model in which complete chemical equilibrium (model CE) is always assumed. This model is employed for the sake of comparison with the other models. We include strange and nonstrange hadrons up to the mass of $\Delta(1232)$. Energy density and pressure are as follows:

$$E = \sum_i \frac{d_i}{(2\pi)^3} \int d^3\boldsymbol{p} \frac{\sqrt{\boldsymbol{p}^2+m_i^2}}{\exp[(\sqrt{\boldsymbol{p}^2+m_i^2}-\mu_i)/T] \mp 1}, \quad (1)$$

$$P = \mp \sum_i T \frac{d_i}{(2\pi)^3} \int d^3\boldsymbol{p} \ln\{1 \mp \exp[-(\sqrt{\boldsymbol{p}^2+m_i^2}-\mu_i)/T]\}, \quad (2)$$

where $\mu_i = 0$ due to complete chemical equilibrium in this model. Here the upper and lower signs correspond to bosons and fermions. We neglect the excluded volume correction which largely affects the hadronic EOS in the high baryon density region. From the Gibbs's equilibrium condition at $T_c = 170$ MeV, we obtain the bag constant $B^{1/4} = 247.2$ MeV and the latent heat $\Delta E \sim 1.7$ GeV/fm^3.

B. Chemical freeze-out

The second model is the simplest one which describes the picture of chemical freeze-out (model CFO). Below $T^{\rm ch}$, we

assume that the numbers of *all* hadrons N_i included in the EOS are fixed and that the particle number densities obey $\partial_\mu n_i^\mu = 0$. We introduce a chemical potential $\mu_i(T)$ associated with each species so that N_i becomes a conserved quantity. From the conservation of entropy $\partial_\mu s^\mu = 0$, the ratio of the particle number density to the entropy density below the chemical freeze-out temperature obeys

$$\frac{n_i(T,\mu_i)}{s(T,\{\mu_i\})} = \frac{n_i(T_{\rm ch},\mu_i=0)}{s(T_{\rm ch},\{\mu_i\}=0)} \tag{3}$$

for all hadrons along the adiabatic path. Here we assume $T^{\rm ch}=170$ MeV, which is consistent with a recent analysis based on a thermal model at the RHIC energy [24]. From Eq. (3), we obtain a chemical potential as a function of temperature for each hadron. The $\mu_i(T)$ ensures keeping the ratios of the number of each hadron throughout the space-time evolution of a fluid element without explicitly solving $\partial_\mu n_i^\mu = 0$. All chemical potentials are functions of temperature, so the thermodynamical variables depend only on temperature even after chemical freeze-out.

C. Partial chemical equilibrium

The third model represents a more realistic EOS than the second one. The following model is first discussed in Ref. [37]. The observed particle numbers are always composed of the contribution from direct particles and resonance decays, i.e., $\overline{N}_\pi = N_\pi + \Sigma_{i\neq\pi}\tilde{d}_{i\to\pi}N_i$. Here $\tilde{d}$ is an effective degree of freedom which is a product of the degeneracy d and the branching ratio B. So some elastic processes with large cross sections (e.g., $\pi\pi\to\rho\to\pi\pi$, $\pi N\to\Delta\to\pi N$, $\pi K\to K^*\to\pi K$) can be equilibrated even below $T^{\rm ch}$ [38] as long as the equality

$$\frac{\overline{n}_i(T,\mu_i)}{s(T,\{\mu_i\})} = \frac{\overline{n}_i(T_{\rm ch},\mu_i=0)}{s(T_{\rm ch},\{\mu_i\}=0)} \tag{4}$$

is kept instead of Eq. (3). We regard π, K, η, N, Λ, and Σ as "stable" particles[1] and that all chemical potentials can be represented by chemical potentials associated with these stable particles, e.g., $\mu_\rho = 2\mu_\pi$, $\mu_{K^*} = \mu_\pi + \mu_K$, $\mu_\Delta = \mu_\pi + \mu_N$, and so on. Thus the third model describes the *partial* chemical equilibrium (model PCE) even below $T^{\rm ch}$ [37]. It should be noted that, after chemical freeze-out, $\mu_N = \mu_{\overline{N}}$ $(\neq 0)$ with keeping baryonic chemical potential $\mu_{\rm B}=0$ in our model.

The model PCE employed here is not the only one to describe the partial chemical equilibrium. There may be other choices for stable particles or other processes to be equilibrated in this model. Various models should be checked by future precise experimental data of particle ratios.

[1]Here we use a term "stable" when the lifetime of a hadron is much longer than that of the fluid (~ 10 fm/c).

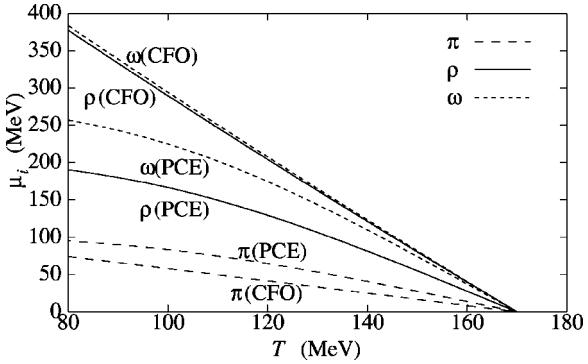

FIG. 1. Chemical potentials for pions (dashed lines), ρ mesons (solid lines), and ω mesons (dotted lines) for the models CFO and PCE.

D. Chemical potentials and equations of state

Figure 1 shows the chemical potentials for π, ρ, and ω mesons for the models CFO and PCE. The difference of chemical potentials between hadrons depends only on their mass in the model CFO, so $\mu_\omega(T)$ behaves like $\mu_\rho(T)$ due to the small mass difference. Both are almost linearly increasing with decreasing temperature. On the other hand, these chemical potentials differ from each other in the model PCE. This results from each elementary process, i.e., $\rho\leftrightarrow\pi\pi$ $(\mu_\rho = 2\mu_\pi)$ and $\omega\leftrightarrow\pi\pi\pi$ $(\mu_\omega = 3\times 0.88\mu_\pi)$, where the branching ratios are from Ref. [39].

One can easily evaluate EOS's for these models by inserting chemical potentials obtained above into Eqs. (1) and (2). We represent pressure and temperature as functions of energy density for three models in Fig. 2. We find in Fig. 2(a) that pressure as a function of energy density is similar. On

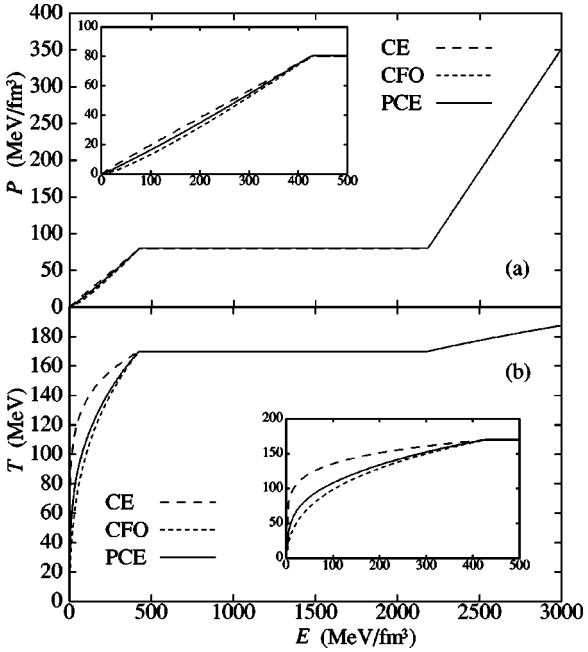

FIG. 2. (a) Pressure as a function of energy density. (b) Temperature as a function of energy density. The dashed, dotted, and solid lines correspond to the models CE, CFO, and PCE.

the other hand, temperature as a function of energy density in the models CFO or PCE in Fig. 2(b) deviates from the model CE. Since the resonance population of the models CFO or PCE is larger than that of the model CE due to the chemical freeze-out, the energy density at a fixed temperature in the hadron phase is also large in those models. Conversely, temperature in the models CFO or PCE at a fixed energy density is *smaller* than in the model CE. This fact is very important in qualitatively understanding the difference of the space-time evolution of fluids among three models as shown in Sec. IV.

III. INITIAL CONDITIONS

We numerically solve the hydrodynamic equation in the full three-dimensional Bjorken coordinate (τ, η_s, x, and y) which is relevant to analyze heavy-ion collisions at the collider energies. Here $\tau=\sqrt{t^2-z^2}$ and $\eta_s=(1/2)\ln[(t+z)/(t-z)]$ are the proper time and the space-time rapidity, respectively. The x axis is parallel to the impact parameter vector and the y axis is perpendicular to the x axis in the transverse plane. As was pointed out in Ref. [6], the main reason to employ the Bjorken coordinate rather than the Cartesian coordinate is a practical one: This considerably reduces numerical efforts such as the long lifetime of fluids (~ 100 fm/c) and less numerical accuracy near the light cone. In addition to this reason, there is also a physical reason why we avoid employing the Cartesian coordinate. When one simulates the space-time evolution in the Cartesian coordinate, one gives the initial condition at a constant t_0. If t_0 is regarded as the thermalization time, this initial condition implies that the thermalization occurs first from the forward (backward) space-time rapidity in the τ-η_s coordinate.[2] This is somewhat unrealistic because the multiplicity in the forward rapidity region is much smaller than the one at midrapidity. This may cause a crucial problem when one discusses the rapidity dependence of radial and elliptic flows at the collider energies, since they are sensitive to the thermalization of the system.

We choose initial conditions in the Bjorken coordinate so as to reproduce the pseudorapidity distribution in Au +Au 130A GeV central (0–6 %) collisions obtained by the PHOBOS Collaboration [40]. At the initial time $\tau_0=0.6$ fm/c, the initial energy density for central collisions can be factorized as

$$E(x,y,\eta_s)=E_{\max}W(x,y;b)H(\eta_s). \tag{5}$$

We assume the transverse profile function $W(x,y;b)$ scales with the impact parameter b in proportion to the number of binary collisions [41],

$$W(x,y;b)\propto T_+T_-, \quad T_\pm=T(x\pm b/2,y), \tag{6}$$

where $T(x,y)$ is a thickness function with the standard Woods-Saxon parametrization for nuclear density,

$$T(x,y)=\int dz\rho(x,y,z),$$

$$\rho(x,y,z)=\frac{\rho_0}{\exp[(\sqrt{x^2+y^2+z^2}-R_0)/\delta]+1}. \tag{7}$$

Here $\rho_0=0.17$ fm^{-3} is the saturation density, $\delta=0.54$ fm is the diffuseness parameter, and $R_0=1.12A^{1/3}-0.86A^{-1/3}$ fm is the nuclear radius. The proportional constant in Eq. (6) is fixed from the condition $W(0,0;0)=1$. The longitudinal profile function $H(\eta_s)$ is characterized by two parts [6,13,42]: it is flat near $\eta_s\sim 0$ and smoothly connects to a vacuum as a half part of the Gauss function in the forward and backward space-time rapidity regions:

$$H(\eta_s)=\exp\left[-\frac{(|\eta_s-\eta_{s0}|-\eta_{\rm flat}/2)^2}{2\eta_{\rm Gauss}^2}\theta(|\eta_s-\eta_{s0}|-\eta_{\rm flat}/2)\right]. \tag{8}$$

The length of a flat region $\eta_{\rm flat}$ and the width of the Gauss function $\eta_{\rm Gauss}$ are adjustable parameters to be determined by the experimental data, especially the (pseudo)rapidity distribution. In symmetric collisions with the vanishing impact parameter, we expect the symmetry $E(x,y,-\eta_s)=E(x,y,\eta_s)$ holds at the initial time. On the other hand, in noncentral (or asymmetric) collisions, we can shift the energy density by η_{s0} which is identified with the center of rapidity for each transverse coordinate [43],

$$\eta_{s0}(x,y;b)=\frac{1}{2}\ln\left[\frac{(T_-+T_+)\gamma_N+(T_--T_+)\gamma_N v_N}{(T_-+T_+)\gamma_N-(T_--T_+)\gamma_N v_N}\right], \tag{9}$$

where v_N and γ_N are, respectively, the velocity and Lorentz γ factor of an incident nucleon in the center-of-mass system. For illustrations of the initial energy density, see Ref. [6]. The initial longitudinal flow is the Bjorken's solution [44], i.e., the fluid rapidity $Y_f(\tau_0)$ is equal to the space-time rapidity η_s. It should be noted that this is merely an initial condition and that $Y_f\neq\eta_s$ after an initial time due to the pressure gradient directed to the η_s axis. The transverse velocities vanish at τ_0 and are to be generated only by the transverse pressure gradient.

Initial parameters in hydrodynamic simulations are chosen as follows: $E_{\max}=35$ GeV/fm^3, $\eta_{\rm flat}=5.8$, $\eta_{\rm Gauss}=0.2$, and $b=2.4$ fm. These values lead us to reproduce the pseudorapidity distribution in Au + Au central collisions at $\sqrt{s_{NN}}=130$ GeV observed by the PHOBOS collaboration [40]. The parameters are adjusted for the model PCE with $T^{\rm th}=140$ MeV. We also use the same values for the other model EOS's for the sake of comparison, although this causes the pseudorapidity distribution to be slightly deviated from the experimental data.

[2]Supposing $t_0=1$ fm/c, the corresponding initial *proper* time becomes $\tau_0=t_0/\gamma_N\sim 0.01$ fm/c near the beam rapidity region at RHIC energies.

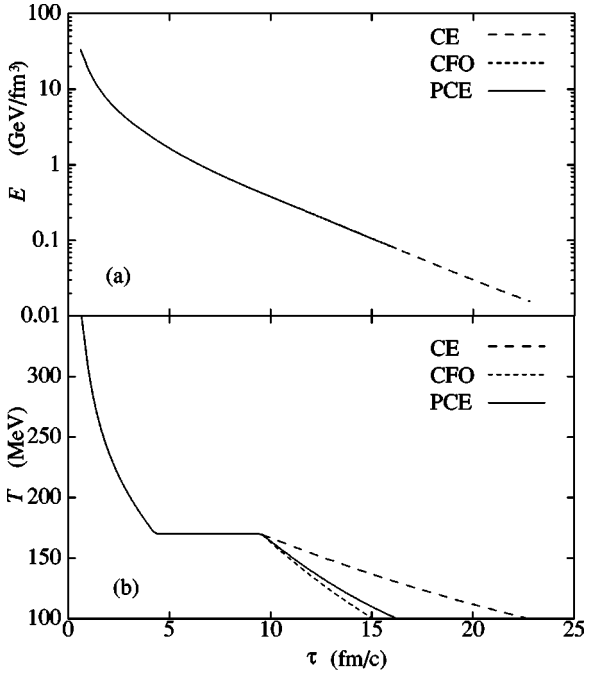

FIG. 3. (a) Time evolution of energy density at the center of the fluid. (b) Time evolution of temperature at the center of the fluid. The dashed, dotted, and solid lines correspond to the models CE, CFO, and PCE.

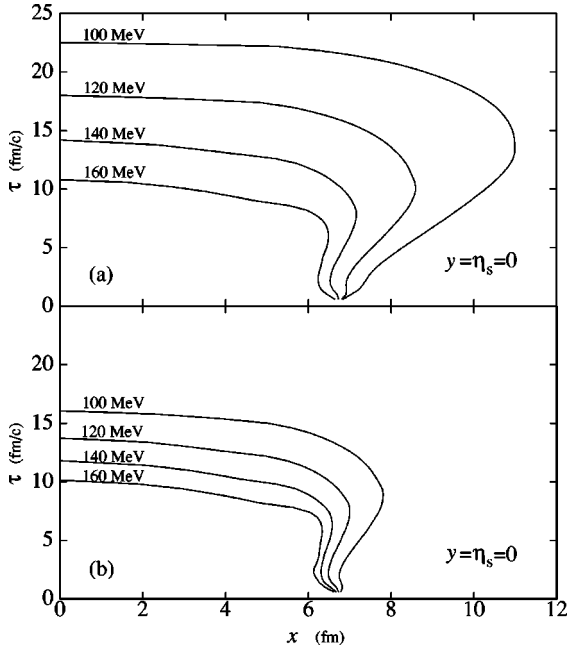

FIG. 4. Space-time evolution of thermal freeze-out hypersurface for (a) the model CE and (b) the model PCE.

IV. TIME EVOLUTION OF FLUIDS

We simulate the space-time evolution of the fluid in the *full* three dimensional space [6] with the initial conditions and the EOS's discussed in the previous sections. First, we pick up a fluid element at the central point ($x=y=\eta_s=0$) and pursue its time evolution until its temperature reaches $T=100$ MeV. Figure 3 shows the time evolution of [Fig. 3(a)] energy density and [Fig. 3(b)] temperature at the center of the fluid for three model EOS's. As far as the time evolution of energy density, we cannot distinguish them. This is easily understood by Fig. 2(a): Energy density evolution is completely governed by the EOS, i.e., $P(E)$ and the three models are very similar to each other. We transform these results from energy density to temperature by using Fig. 2(b). For the time evolution of temperature, chemical freeze-out makes a substantial difference between the model CE and the model CFO or PCE. If we suppose thermal freeze-out occurs at the constant temperature, the system in which the property of the chemical freeze-out is considered is destined to be thermally frozen earlier than the conventional model CE. The early chemical freeze-out makes the hadron phase cool down more rapidly [45].

Next, we show how the early chemical freeze-out affects the spatial size of the fluid. Figure 4 represents the time evolution of freeze-out hypersurfaces at $y=\eta_s=0$ for [Fig. 4(a)] the model CE and [Fig. 4(b)] the model PCE. Here the hypersurfaces in Fig. 4 correspond to various $T^{\rm th}=100$, 120, 140, and 160 MeV which are within a plausible range for the thermal freeze-out temperature. We find that the early chemical freeze-out reduces not only the lifetime of the fluid but also its spatial size and that the fluid does not expand so explosively for the model PCE. Since the two-particle correlation function is sensitive to the spatial size and the lifetime of the fluid, it is interesting to see the effect of early chemical freeze-out on the HBT radii. Detailed analyses of pion interferometry will be discussed in Sec. VI.

Figure 5 shows the thermal freeze-out temperature dependencies of average radial flow at midrapidity $\langle v_r\rangle|_{\eta_s=0}$, where $v_r=\sqrt{v_x^2+v_y^2}$. Radial flow is generated by the pressure gradient, so it contains information about the EOS. From this figure, the radial flow is suppressed when we take account of the early chemical freeze-out. At $T^{\rm th}=140(120)$ MeV, the average radial flow for the model PCE is reduced by 17.7% (22.5%) from the one for the conventional model CE.

It should be noted that the difference between the thermal freeze-out temperature $T^{\rm th}$ and the thermal freeze-out energy density $E^{\rm th}$ plays an important role in analyses of particle spectra. It may be claimed that there are no significant dif-

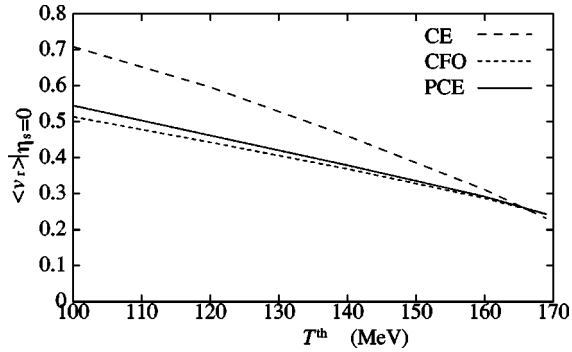

FIG. 5. Thermal freeze-out temperature dependence of average radial flow. The dashed, dotted, and solid lines correspond to the models CE, CFO, and PCE.

ferences among three models when one shows the results in Figs. 4 and 5 as functions of the thermal freeze-out *energy density* $E^{\rm th}$, not temperature $T^{\rm th}$. It is indeed true when one discusses only the hydrodynamic behavior. The shape of particle distributions, especially the p_t spectrum, are determined by the thermal freeze-out *temperature* $T^{\rm th}$ and the flow in the hydrodynamic model. So this difference is clearly meaningful when we compare the numerical results of particle spectra with experimental data as shown in the next section.

V. SINGLE-PARTICLE SPECTRA AND AZIMUTHAL ASYMMETRY

Hydrodynamics has a limited prediction power, so the calculation is really meaningful only after tuning the initial parameters and reproducing the single-particle spectra. The momentum distribution for particles directly emitted from a (thermal) freeze-out hypersurface can be calculated through the Cooper-Frye formula [46]

$$E\frac{dN}{d^3\boldsymbol{p}} = \frac{d}{(2\pi)^3}\int_\Sigma \frac{p\cdot d\sigma}{\exp[(p\cdot u-\mu_i)/T^{\rm th}]\mp 1}. \qquad (10)$$

Here, Σ and $d\sigma^\mu$ are the thermal freeze-out hypersurface and its element. u^μ is the four fluid velocity. The $-$ $(+)$ sign is for boson (fermion) and d is the degeneracy of particles under consideration. This formula merely counts the net particles passing through the hypersurface Σ rather than decoupling from the system. Although it has a problem with the negative number in the treatment of the timelike freeze-out hypersurface [47], this is widely used in almost all hydrodynamic models. The observed spectra always contain the contribution from resonance decays. We assume all of the resonance particles in the EOS are also emitted from a freeze-out hypersurface and that they decay into stable particles. Taking account of the decay kinematics, we easily obtain the single-particle spectra from resonance particles [31,32].[3] For further details to calculate the spectra from resonance decays, see the Appendix. Since the results from the model CFO are similar to the ones from the model PCE, we hereafter concentrate our discussions on the models CE and PCE.

A. Spectra and flow for charged hadrons

Figure 6 shows the pseudorapidity distribution of charged particles in Au + Au 130*A* GeV collisions. We choose $T^{\rm th}=140$ MeV for both models. From the analyses based on the wounded nucleon model, we choose the impact parameter $b=2.4$ fm for 0–6 % central collisions and $b=8.9$ fm for 35–45 % noncentral collisions. The resultant number of participants is 342 (94) for $b=2.4$ (8.9) fm, which is consistent with estimation by the PHOBOS Collaboration [40]. We reasonably reproduce the data in not only central but also noncentral collisions by using initial parameters in the previous section. After tuning initial parameters for central events, we have no adjustable parameters for noncentral events due to assuming the binary collision scaling. For noncentral collisions, we change the impact parameter in Eq. (6) as to the number of participants and keep other parameters in the initial condition. Although the binary collisions contribute to hard components, the binary collision scaling seems to be reasonable to parametrize the hydrodynamic initial condition [41] from Fig. 6.

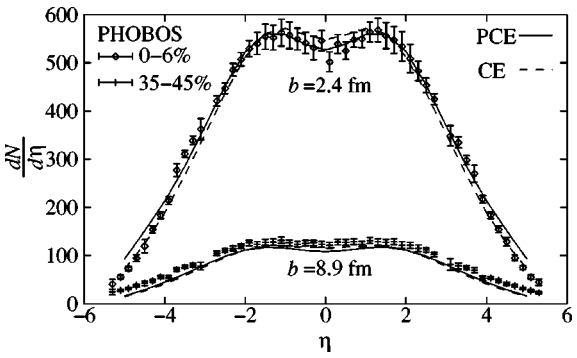

FIG. 6. Pseudorapidity distribution of charged particles in Au+Au 130*A* GeV central and semicentral collisions. Data from Ref. [40].

We next show in Fig. 7 the p_t spectrum for negative charged hadrons. The experimental data (0–5 % central [48] and 30–40 % semicentral events [49]) are observed by the STAR Collaboration. The impact parameters used in this calculation are $b=2.4$ fm for central and $b=8.6$ fm for semi central events. We represent the thermal freeze-out temperature dependence of the p_t spectrum for the models CE and PCE. The slope of p_t spectrum is almost independent of $T^{\rm th}$

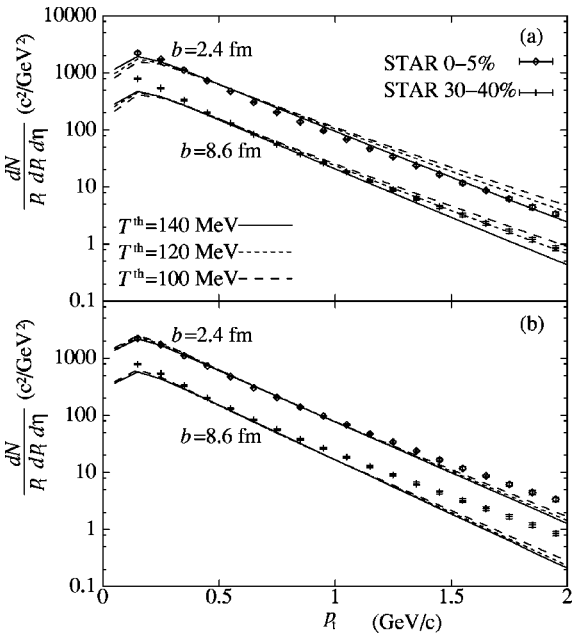

FIG. 7. Transverse momentum spectra of negative charged particles in Au+Au 130*A* GeV central and semicentral collisions for (a) the model CE and (b) the model PCE. The dashed, dotted, and solid lines correspond to $T^{\rm th}=100$, 120, and 140 MeV. Data from Refs. [48,49].

[3]When we calculate the two-pion correlation function in the next section, we neglect this contribution for simplicity.

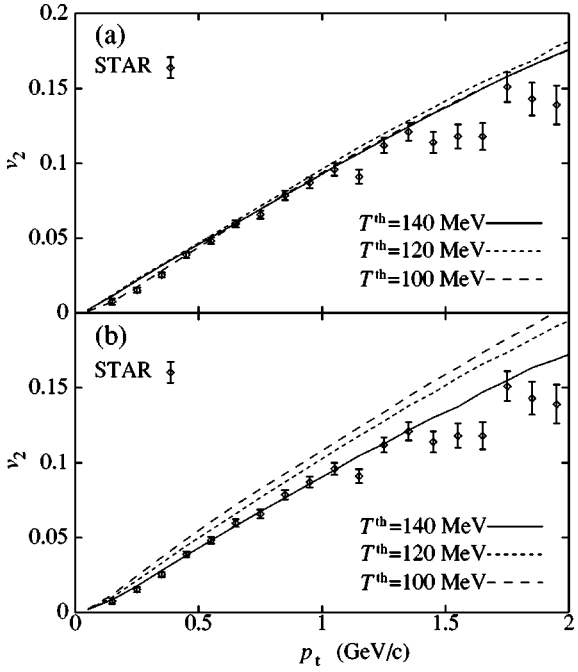

FIG. 8. $v_2(p_t)$ for charged hadrons in Au+Au 130*A* GeV collisions. The dashed, dotted, and solid lines correspond to $T^{\mathrm{th}}=100$, 120, and 140 MeV. Data from Ref. [50].

near $p_t \sim 1$ GeV/c, which is a little peculiar in the usual sense. However, it is interpreted by the result in Fig. 5. When one reduces the thermal freeze-out temperature by hand, the average radial flow enhances as its response. The magnitude of the response is governed by the EOS. The resultant p_t slope is a competition between these two effects: The reduction of temperature makes the slope steeper in the case of vanishing flow, while the thermal distribution is Lorentz-boosted by radial flow, and the p_t slope becomes flatter. The effect of generated radial flow on the p_t slope usually overcomes that of the reduction of T^{th} in the model CE, so the p_t slope becomes flatter with decreasing T^{th}. On the other hand, the radial flow is slightly suppressed in the model PCE as shown in Fig. 5. Hence the reduction of T^{th} is just compensated by its response to radial flow for the model PCE. This is the reason why the p_t slope is almost independent of T^{th} in Fig. 7. For the model CE, we reproduce the slope by choosing $T^{\mathrm{th}}=140$ MeV. For the model PCE, in any T^{th} within a plausible range, we reproduce the experimental data below 1 GeV/c for central collisions. This indicates that there exists the onset of hard processes around $p_t \sim 1$ GeV/c. It should be noted that a bend of the spectrum in the low p_t region is simply due to the Jacobian between the pseudorapidity η and the rapidity Y.

We next show the transverse momentum dependence of the second Fourier coefficient for azimuthal distribution for the models CE and PCE. Figure 8 represents $v_2(p_t)$ for charged particles in minimum bias collisions. Experimental data is also observed by STAR [50]. Hydrodynamic analysis of the data has already been done by Kolb *et al.* [51]. They found the hydrodynamic result excellently coincides with the data below $p_t \sim 1.5$ GeV/c. Our results for the model CE are

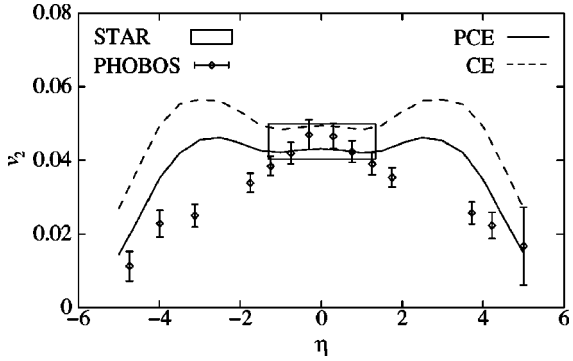

FIG. 9. $v_2(\eta)$ for charged hadrons in Au+Au 130*A* GeV collisions. The solid and dashed lines correspond to the models PCE and CE. Data from Refs. [50,53].

consistent with their results. Now that we find the space-time evolution in our model is different from their result where chemical equilibrium is always assumed, we must check whether the hydrodynamic description is really accurate at RHIC even when we include the effects of early chemical freeze-out. The numerical results are calculated from the following equation:

$$v_2(p_t)=\frac{\sum_b \int d\eta d\phi \cos(2\phi) b \frac{dN}{p_t dp_t d\eta d\phi}(p_t,\eta,\phi;b)}{\sum_b \int d\eta b \frac{dN}{p_t dp_t d\eta}(p_t,\eta;b)}. \tag{11}$$

Here the summation with respect to the impact parameter b is taken over every 2 fm up to 14 fm in this analysis. The integral region of η is from -1.3 to 1.3, which corresponds to the analysis by STAR [50]. The value of $v_2(p_t)$ depends on the thermal freeze-out temperature T^{th} in contrast with the p_t spectrum. We also reproduce the experimental data below 1 GeV/c by choosing $T^{\mathrm{th}}=140$ MeV and slightly overestimate the data above 1 GeV/c. Similar to the p_t spectrum, this result also indicates that the hard contribution, which reduces v_2 calculated from the hydrodynamic source [5,52], becomes important above 1 GeV/c.

In Fig. 9, we compare the pseudorapidity dependence of elliptic flow between the models CE and PCE. Similar to the $v_2(p_t)$, $v_2(\eta)$, which is to be compared with minimum bias data, is

$$v_2(\eta)=\frac{\sum_b \int p_t dp_t d\phi \cos(2\phi) b \frac{dN}{p_t dp_t d\eta d\phi}(p_t,\eta,\phi;b)}{\sum_b \int p_t dp_t b \frac{dN}{p_t dp_t d\eta}(p_t,\eta;b)}. \tag{12}$$

We choose $T^{\mathrm{th}}=140$ MeV and integrate with respect to p_t from 0 to 2.0 GeV/c. Data plots are observed by PHOBOS [53]. The rectangular area corresponds to the statement by STAR [50], $v_2(\eta)=4.5\pm 0.5\%$ for $0.1<p_t<2.0$ GeV/c and $|\eta|<1.3$. As for the case of radial flow, the elliptic flow is also reduced by taking account of the chemical freeze-out.

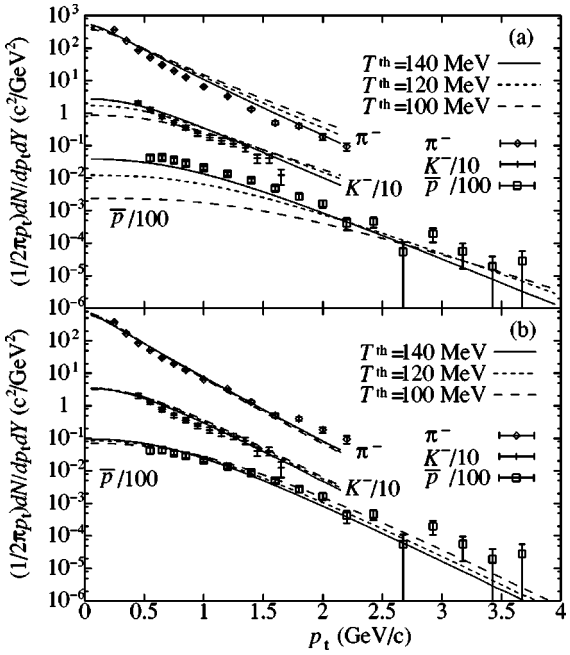

FIG. 10. The transverse momentum spectra for negative pions, negative kaons, and antiprotons for (a) the model CE and (b) the model PCE. To see these results clearly, the yield of kaons (antiprotons) is scaled by 10^{-1} (10^{-2}). The dashed, dotted, and solid lines represent results for $T^{\rm th}=100$, 120, and 140 MeV, respectively. Data from Ref. [36].

We reproduce the PHOBOS data only near mid-(pseudo-) rapidity and overestimate in forward and backward rapidity. On the other hand, a microscopic transport model reproduces the data only in forward and backward rapidity regions [54]. This indicates that the full thermalization is achieved only near midrapidity, although there are some open problems in hydrodynamics such as the treatment of freeze-out through the Cooper-Frye formula, more sophisticated initialization, and the absorption by spectators [6].

From Figs. 8 and 9, the hydrodynamic description with early chemical freeze-out seems to be valid for, at least, $0<p_t<1$ GeV/c and $-1<\eta<1$ in Au+Au collisions at 130A GeV.

B. Spectra and Flow for Identified Hadrons

In this subsection, let us see the difference between the models CE and PCE by comparing p_t spectra and $v_2(p_t)$ for *identified* hadrons which are supposed to be sensitive to the early chemical freeze-out.

The p_t spectra for identified hadrons in (0–5 %) central collisions observed by the PHENIX Collaboration [36] are compared with our results in Fig. 10. The impact parameter which we choose for central collisions is also $b=2.4$ fm. For the model CE, the slopes of pions, kaons, and antiprotons become steeper with increasing $T^{\rm th}$, which is similar to the case of charged particles. The number of antiprotons becomes very small at $T^{\rm th}=100$ MeV for the model CE due to chemical equilibrium. On the other hand, the numbers of each hadron in the model PCE are independent of $T^{\rm th}$ and reasonably agree with experimental data. The number of antiprotons in the model PCE might be slightly improved by taking into account the baryonic chemical potential which is neglected in the present analysis. It should be noted that pion spectra in the large p_t (>1.5 GeV/c) region can be reproduced by including contributions from nonthermalized hard partons (jets) with energy loss [55].

We next show in Fig. 11 the elliptic flow, for identified hadrons, and its $T^{\rm th}$ dependence. The STAR data [56] are

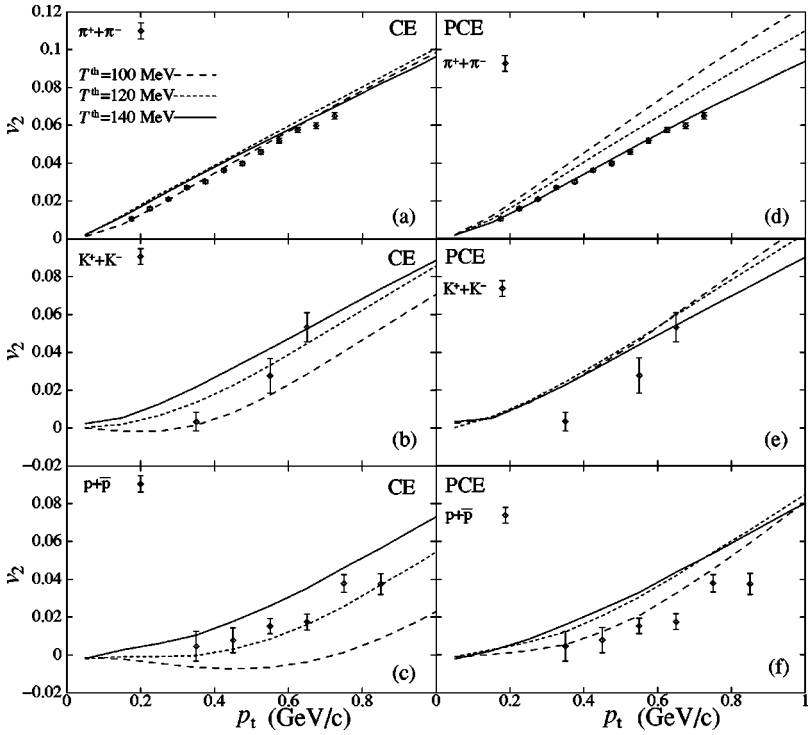

FIG. 11. $v_2(p_t)$ for pions, kaons, and protons in Au + Au 130A GeV collisions. Left (right) column represents the results for the model CE (PCE). Data from Ref. [56].

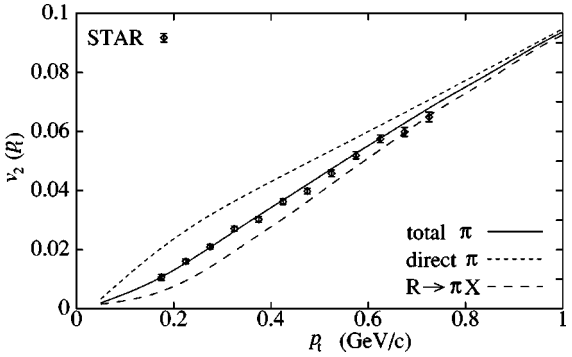

FIG. 12. $v_2(p_t)$ for charged pions. The solid, dotted, and dashed lines correspond to total pions, pions directly emitted from freeze-out hypersurface, and pions from resonance decays. Data from Ref. [56].

compared with our results with or without chemical equilibrium. For the model CE, $v_2(p_t)$ of pions is almost independent of $T^{\rm th}$, while $v_2(p_t)$ of kaons and protons increases with $T^{\rm th}$. On the other hand, v_2 of pions grows with decreasing $T^{\rm th}$ for the model PCE. Whether $v_2(p_t)$ increases with $T^{\rm th}$ depends not only on the particle mass but also on the flow velocities and its anisotropy in the transverse plane [57]. The elliptic flow seems to be more sensitive to $T^{\rm th}$ than p_t spectra when we consider the early chemical freeze-out. For the transverse momentum spectra of identified hadrons shown in Fig. 7, we roughly reproduce the slope in the low p_t region with $T^{\rm th}=140$ MeV. On the other hand, we cannot reproduce $v_2(p_t)$ of identified hadrons by a common thermal freeze-out temperature: each hadron seems to favor different $T^{\rm th}$. This indicates that the hadronic afterburner in the late stage of the expansion may be important [58]. From a hydrodynamic point of view, detailed analyses with various EOS's and initial conditions are needed to understand thermal freeze-out properties.

Figure 12 separately represents the contribution of pions directly emitted from the freeze-out hypersurface and the contribution of pions from resonance decays. The STAR data show the contribution from identified pions [56]. From this figure, the concavity of $v_2(p_t)$ in the low p_t region ($p_t < 0.3$ GeV/c) results from the resonance decay after thermal freeze-out. The exact treatment of the decay kinematics of resonances dilutes v_2 for direct pions especially in the low p_t region [32]. The fraction of the contribution from resonance decays plays a very important role in understanding $v_2(p_t)$ for pions in the low p_t region, so the early chemical freeze-out must be included when one discusses the phenomena proper to the low transverse momentum.

VI. PION INTERFEROMETRY

From single-particle spectra and azimuthal asymmetry, we obtain information about the distribution in the momentum space at freeze-out. On the other hand, we can obtain information about the particle distribution in the coordinate space through two-particle interferometry [59]. We see in Sec. IV that the space-time evolutions are considerably different between the models with and without chemical equilibrium. To see this more clearly, we discuss the two-pion correlation function in this section.

In hydrodynamics, the two-particle correlation function for directly emitted bosons from the freeze-out hypersurface Σ can be calculated from [60,61]

$$C_2(\boldsymbol{p}_1,\boldsymbol{p}_2) = \frac{P(\boldsymbol{p}_1,\boldsymbol{p}_2)}{P(\boldsymbol{p}_1)P(\boldsymbol{p}_2)} = 1+\frac{\left|\frac{d}{(2\pi)^3}\int_\Sigma K\cdot d\sigma \exp(ix\cdot q) f_{\rm BE}\left(\frac{K\cdot u-\mu_i}{T^{\rm th}}\right)\right|^2}{E_1\frac{dN}{d^3\boldsymbol{p}_1}E_2\frac{dN}{d^3\boldsymbol{p}_2}}. \tag{13}$$

Here $P(\boldsymbol{p}_1,\boldsymbol{p}_2)$ is the two-particle coincidence cross section and $P(\boldsymbol{p}_1)$ is the same Cooper-Frye formula represented in Eq. (10). We consider only directly emitted pions for simplicity. $K^\mu=(p_1^\mu+p_2^\mu)/2$ and $q^\mu=p_1^\mu-p_2^\mu$ are, respectively, the average and relative four momentum of the pair. $f_{\rm BE}=(e^x-1)^{-1}$ is the Bose-Einstein distribution function. The information about hydrodynamic simulations enter through the freeze-out hypersurface Σ and the four velocity u^μ in this equation. The average pair momentum K is decomposed into the transverse momentum K_T, the longitudinal momentum K_z, and the azimuthal angle Φ_K.[4] The relative pair momentum q^μ is also decomposed into the standard coordinate, $q_{\rm out}$ (parallel to K_T), $q_{\rm long}$ (along the beam direction), and $q_{\rm side}$ (perpendicular to the others). Since the experimental acceptances are limited to midrapidity, $|Y|<0.5$ (STAR) [62] or $|\eta|<0.35$ (PHENIX) [63], we can put $K_z=0$. Moreover, we average the two-particle function C_2 over the azimuthal angle Φ_K. Thus we obtain the following equation which can be compared with the experimental data:

$$C_2(K_T,q_{\rm side},q_{\rm out},q_{\rm long}) = \left.\frac{\int \Phi_K P(\boldsymbol{p}_1,\boldsymbol{p}_2)}{\int \Phi_K P(\boldsymbol{p}_1)P(\boldsymbol{p}_2)}\right|_{K_z=0}. \tag{14}$$

Our definition of the HBT radii is similar to the one used in Refs. [61,64,65]. Assuming that $C_2(K_T,q_{\rm side},q_{\rm out},q_{\rm long})$ for each K_T is fitted by the Gaussian form

$$C_2 = 1+\lambda\exp(-R_{\rm side}^2 q_{\rm side}^2 - R_{\rm out}^2 q_{\rm out}^2 - R_{\rm long}^2 q_{\rm long}^2) \tag{15}$$

with a chaoticity $\lambda=1$, the K_T dependence of the HBT radius for the side direction is $R_{\rm side}(K_T)=1/q^*_{\rm side}(K_T)$, where

[4]Even for central events, we no longer have cylindrical symmetry around the collision axis due to the small (but finite) value of the impact parameter, so C_2 depends on the azimuthal angle Φ_K which is measured from the reaction plane.

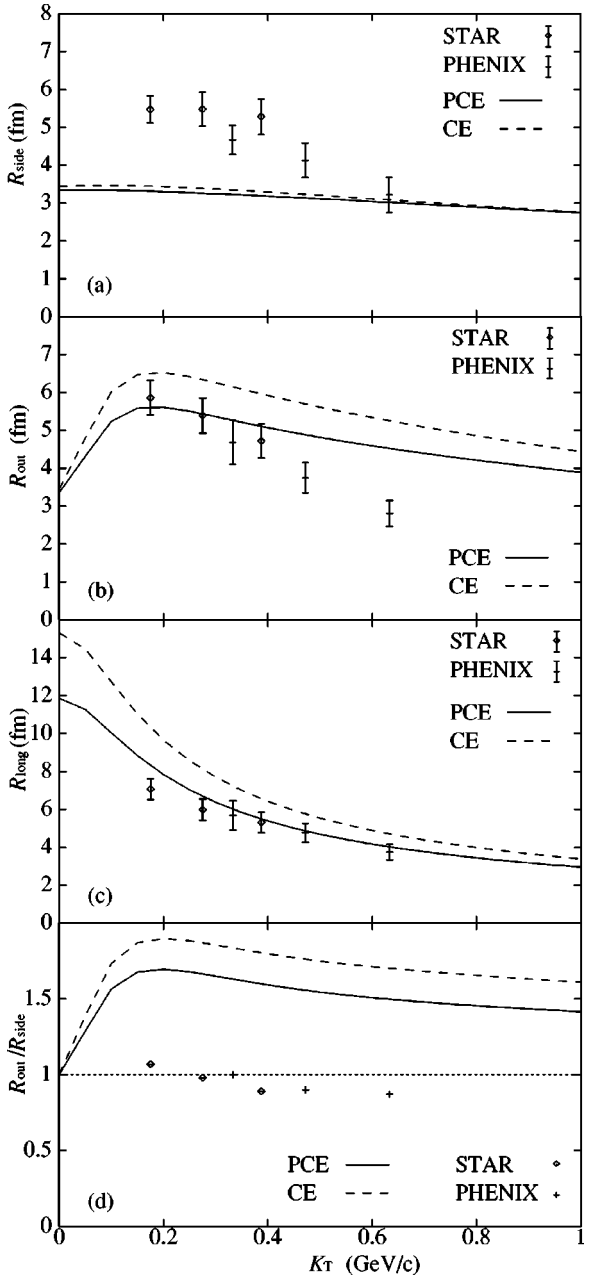

FIG. 13. HBT radii for negative pions in (a) side, (b) out, and (c) long directions and (d) its ratio $R_{\rm out}/R_{\rm side}$ as a function of K_T. The solid and dashed lines correspond to the models PCE and CE. Data from Refs. [62,63].

$C_2(K_T,q^*_{\rm side},0,0)=1+e^{-1}$, and analogous definitions are used for the K_T dependence of $R_{\rm out}$ and $R_{\rm long}$.

We evaluate two-pion correlation functions for negative pions directly emitted from the freeze-out hypersurface and obtain the K_T dependence of $R_{\rm side}$, $R_{\rm out}$, and $R_{\rm long}$. Figure 13 shows the HBT radii and the ratio $R_{\rm out}/R_{\rm side}$ for the models CE and PCE with $T^{\rm th}=140$ MeV. Here the impact parameter which we choose in this analysis is $b=2.4$ fm. The difference between the two models is very small for $R_{\rm side}$. On the other hand, $R_{\rm out}$ and $R_{\rm long}$ for the model PCE are significantly smaller than the ones for the model CE, which reflects the space-time evolution of the freeze-out hypersurface depicted in Fig. 4. We compare our results with experimental data observed by STAR (12% most central events) [62] and PHENIX (30% most central events) [63]. We reproduce the K_T dependence of $R_{\rm long}$ by employing the model PCE, while $R_{\rm side}$ and $R_{\rm out}$ do not show good agreement with the experimental data.

It has been suggested that the ratio $R_{\rm out}/R_{\rm side}$ reflects the prolongation of the lifetime due to the phase transition between the QGP phase and the hadron phase [61]. Various models predict that this ratio has a value significantly larger than unity in some K_T regions [42,61,64–66], although it is around unity in $0.2<K_T<0.6$ GeV/c in Au + Au $\sqrt{s_{NN}}=130A$ GeV collisions according to the recent measurement at RHIC [62,63]. This discrepancy is often called the ''HBT puzzle'' [66,67]. The ratio for the model PCE reduces by about 12% above 0.2 GeV/c due to the property of the early chemical freeze-out, but it clearly turns out to be larger than the experimental data. Our aim in this paper is to see how the early chemical freeze-out affects the HBT radii, so we leave detailed discussions on the HBT puzzle for future works.[5]

VII. SUMMARY AND DISCUSSION

We have investigated the effect of early chemical freeze-out on the hydrodynamic evolution and the particle spectra by using a genuine three dimensional hydrodynamic model. We constructed the equation of state for hadronic matter which is in partial chemical equilibrium. Pressure as a function of energy density is not affected by the chemical non-equilibrium property, while temperature as a function of energy density is largely reduced due to the large population of resonance particles. By using the EOS with a first order phase transition, we simulated hydrodynamic evolution at the RHIC energy. We found the system cools more rapidly than the conventional model and that the lifetime and the spatial size of the fluid and the radial and elliptic flows are reduced when they are compared at the isothermal hypersurface. We also analyzed particle spectra and two-pion correlation functions in Au+Au 130*A* GeV collisions. We chose initial parameters in the hydrodynamic simulations so as to reproduce the pseudorapidity distribution in central collisions observed by PHOBOS. The slope of the p_t spectrum for negative hadrons is less sensitive to the thermal freeze-out temperature, which results from the reduction of radial flow. On the other hand, the transverse momentum dependence of elliptic flow $v_2(p_t)$ for charged hadrons depends on the thermal freeze-out temperature. The situation is completely opposite to the ordinary hydrodynamic results. In the conventional models, the p_t slope is steeper with increasing $T^{\rm th}$ and $v_2(p_t)$ is not so sensitive to $T^{\rm th}$. We found $T^{\rm th}=140$ MeV and the resultant average radial flow $\langle v_r\rangle$

[5]In Ref. [42], slightly larger $R_{\rm side}$ is obtained by assuming a simple flat transverse profile and vanishing impact parameter for initial energy density distribution. The flat profile leads a larger value of the root-mean-square radius of a fluid in the transverse plane than that of the present initialization based on the binary collision scaling.

$=0.38c$ are the values to simultaneously reproduce the p_t slope and $v_2(p_t)$ for charged hadrons (mainly pions) below 1 GeV. $v_2(\eta)$ is also reduced by the early chemical freeze-out, but we failed to reproduce the data in forward and backward rapidity regions. We see the thermal freeze-out temperature independence of the p_t slope more clearly in the p_t spectra for identified hadrons. We reasonably reproduce the p_t slope with $T^{\rm th}=100$–140 MeV for the model PCE, while $v_2(p_t)$ for identified hadrons seems to favor different thermal freeze-out temperatures which are dependent on hadronic species. In order to see more quantitatively the effect of early chemical freeze-out on the temporal or spatial size of fluids, we calculated the two-pion correlation functions and obtained the HBT radii. By taking account of the early chemical freeze-out in the EOS, $R_{\rm out}$, $R_{\rm long}$, and $R_{\rm out}/R_{\rm side}$ are significantly suppressed, while $R_{\rm side}$ is not changed. Nevertheless, the properties of the early chemical freeze-out are not enough to interpret the HBT puzzle.

It would be very interesting to see other observables in the case of partial chemical equilibrium. Although the best place to see the difference between the models CE and PCE must be the particle ratios, we cannot discuss this observable by using the present model due to an approximation of vanishing baryonic chemical potential. This will be discussed elsewhere. Penetrating probes such as thermal photons and dileptons may also be affected by the early chemical freeze-out. The emission rates of photons or dileptons increase due to the chemical potentials for hadrons, while the space-time volume of the hadron phase decreases. Therefore we should check whether the total multiplicity and spectra of photons and dileptons are changed in terms of hydrodynamics.

There are other approaches to describe the early chemical freeze-out. These models evolve the QGP and mixed phases as a relativistic fluid, while it switches to a hadronic cascade model, e.g., UrQMD [68] or RQMD [58]. The advantage of our hydrodynamic model over these hybrid (hydrodynamics + cascade) models is to be able to obtain the average hydrodynamic behavior and the effect of temperature naturally. When one discusses the spectral changes of hadrons due to the medium effects such as temperature and/or baryonic chemical potential [69], one can easily estimate their effect by using hydrodynamic simulations. We regard the model PCE as a complementary tool to those hybrid models.

After publishing our preliminary results [29] and almost finishing this work, the authors became aware of a paper concerning the same subject [70], in which the conclusion of the hydrodynamic behavior is almost the same as ours. In Ref. [70], the effect of finite baryonic chemical potential is included but the hydrodynamic simulation is performed only in the transverse plane by assuming the Bjorken's scaling solution.

ACKNOWLEDGMENTS

The authors thank members of the high-energy physics group at Waseda University for useful comments and K. Kajimoto for his collaboration in the early stage of this work. One of the authors (T.H.) acknowledges valuable discussions with T. Hatsuda, P. Huovinen, K. Morita, S. Muroya, H. Nakamura, C. Nonaka, and D. Rischke. He also thanks the Inoue Foundation for Science for financial support.

APPENDIX: MONTE CARLO CALCULATION OF THE CONTRIBUTION FROM RESONANCE DECAYS

In this appendix, we show how to calculate the particle distribution from resonance decays within the Cooper-Frye prescription. This method can be used in hydrodynamics-motivated models as well as in hydrodynamics.

Lorentz transformation for the momentum of a decay particle between the local rest system (starred) and the finite momentum system (nonstarred) of a resonance particle R is

$$\boldsymbol{p}^*=\boldsymbol{p}-\boldsymbol{p}_R\left[\frac{E}{m_R}-\frac{\boldsymbol{p}\cdot\boldsymbol{p}_R}{m_R(m_R+E_R)}\right]. \tag{A1}$$

We rewrite Eq. (A1) explicitly

$$p_l^*=p_l-p_{Rl}F(p_l,\phi), \tag{A2}$$

$$\cos\phi^*=\frac{p_x^*}{p_t^*}=\frac{p_t(p_l,\phi)\cos\phi-p_{Rt}\cos\phi_R F(p_l,\phi)}{\sqrt{p_t^2(p_l,\phi)+p_{Rt}^2F^2(p_l,\phi)-2p_t(p_l,\phi)p_{Rt}\cos(\phi-\phi_R)F(p_l,\phi)}}, \tag{A3}$$

where

$$F(p_l,\phi)=\frac{E(p_l,\phi)}{m_R}-\frac{p_t(p_l,\phi)p_{Rt}\cos(\phi-\phi_R)+p_lp_{Rl}}{m_R(m_R+E_R)}. \tag{A4}$$

Here the independent variables which we choose for decay particles are the longitudinal momentum p_l and the azimuthal angle ϕ. Thus the transverse momentum of a decay particle p_t is written in terms of p_l and ϕ,

$$p_t(p_l,\phi)=\frac{1}{\gamma_R[1-v_{Rt}^2\cos^2(\phi-\phi_R)]}\{(E^*+p_lv_{Rl}\gamma_R)v_{Rt}\cos(\phi-\phi_R) \pm\sqrt{(E^*+p_lv_{Rl}\gamma_R)^2-(p_l^2+m^2)\gamma_R^2[1-v_{Rt}^2\cos^2(\phi-\phi_R)]}\}. \tag{A5}$$

The Jacobian of the Lorentz transformation is defined by

$$dp_l^* d\phi^* = J(p_l, \phi; \boldsymbol{V}_R) dp_l d\phi, \tag{A6}$$

$$J(p_l, \phi; \boldsymbol{V}_R) = \begin{vmatrix} \frac{\partial p_l^*}{\partial p_l} & \frac{\partial p_l^*}{\partial \phi} \\ \frac{\partial \phi^*}{\partial p_l} & \frac{\partial \phi^*}{\partial \phi} \end{vmatrix}. \tag{A7}$$

The calculation of J is straightforward, so that we do not represent it here. The normalization of momentum space volume for a decay particle in the resonance rest frame is

$$\int_{-p^*}^{p^*} \frac{dp_l^*}{2p^*} \int_0^{2\pi} \frac{d\phi^*}{2\pi} = 1. \tag{A8}$$

We always average the decay probability over the spin of resonances, so that the decay probability does not depend on p_l^* and ϕ^*. Thus the normalization in the resonance reference frame is

$$\int \frac{J(p_l, \phi; \boldsymbol{V}_R) dp_l d\phi}{4\pi p^*} = 1. \tag{A9}$$

The Jacobian in Eq. (A6) has very narrow peaks when the resonance particle moves at a large velocity in the laboratory system [32]. This singularity makes it difficult to integrate the Jacobian numerically. So we introduce a very simple Monte Carlo calculation to evaluate the momentum distribution from resonance decays. All input parameters in this calculation are the numerical results of hydrodynamic simulation, i.e., the temperature $T^{\rm th}$, the chemical potential for resonance particles μ_R, the three dimensional fluid velocity $\boldsymbol{v}$, and the element $d\sigma^\mu$ on the freeze-out hypersurface Σ. In the following discussion, we show how to obtain the rapidity distribution of negative pions, for simplicity, only from ρ mesons. In this case, the branching ratio $B_{\rho^{0(-)} \to \pi^- \pi^{+(0)}} = 1$. It is straightforward to extend this scheme to the cases for other resonances or the transverse mass (momentum) distribution.

Step 1. Evaluate the number of ρ^0 and ρ^- which are emitted from *or* absorbed by the kth freeze-out hypersurface element $d\sigma_k^\mu$:

$$N_k^R = \frac{g_R}{(2\pi)^3} \int_\Sigma \frac{d^3 p_R}{E_R} \frac{|p_R \cdot d\sigma_k|}{\exp[(p_R \cdot u_k - \mu_R)/T^{\rm th}] - 1}. \tag{A10}$$

The integrand does not contain the Jacobian, so that it is simple to carry out the numerical integration by a standard technique. It should be noted that N_k^R is different from the *net* number of emitted ρ mesons from the kth fluid element and that this is used merely for normalization.

Step 2. Generate $\tilde{N}$ random momenta P_j^* $(1 \leqslant j \leqslant \tilde{N})$ for ρ mesons which obey the distribution

$$\frac{P^{*2}}{\exp[(\sqrt{P^{*2} + m_R^2} - \mu_R)/T^{\rm th}] - 1}. \tag{A11}$$

Here we omit the Breit-Wigner function for simplicity.

Step 3. For each $\tilde{N}$ random momentum P_j^*, generate random variables (Θ_j^*, Φ_j^*) whose ensemble is uniformly distributed on the unit sphere. By using these random variables, we obtain an ensemble of ρ mesons with momentum $\boldsymbol{P}_j^* = (P_{xj}^*, P_{yj}^*, P_{zj}^*) = (P_j^* \sin\Theta_j^* \cos\Phi_j^*, P_j^* \sin\Theta_j^* \sin\Phi_j^*, P_j^* \cos\Theta_j^*)$, which obeys the Bose-Einstein distribution in the fluid rest system.

Step 4. Boost $\boldsymbol{P}_j^*$ with respect to the fluid velocity $\boldsymbol{v}_k$

$$\boldsymbol{P}_j = \boldsymbol{P}_j^* + \boldsymbol{v}_k \gamma_k \left(E_j^* + \frac{\boldsymbol{P}_j^* \cdot \boldsymbol{v}_k \gamma_k}{1 + \gamma_k} \right), \tag{A12}$$

where $\gamma_k = 1/\sqrt{1 - \boldsymbol{v}_k^2}$.

Step 5. Generate $\tilde{N}$ uniform random variables on the unit sphere (θ_j^*, ϕ_j^*) and obtain an ensemble of negative pions with momentum

$$\begin{aligned} \boldsymbol{p}_j^* &= (p_{xj}^*, p_{yj}^*, p_{zj}^*) \\ &= (p^* \sin\theta_j^* \cos\phi_j^*, p^* \sin\theta_j^* \sin\phi_j^*, p^* \cos\theta_j^*), \end{aligned}$$

where p^* is given by

$$p^* = \frac{1}{2m_R} \sqrt{(m_R + m_\pi)^2 - m_X^2} \sqrt{(m_R - m_\pi)^2 - m_X^2}. \tag{A13}$$

For the decay process $\rho \to \pi\pi$, $m_X = m_\pi$.

Step 6. Boost $\boldsymbol{p}_j^*$ with respect to the resonance momentum $\boldsymbol{P}_j$:

$$\boldsymbol{p}_j = \boldsymbol{p}_j^* + \boldsymbol{P}_j \left[\frac{E_j}{m_R} + \frac{\boldsymbol{p}_j^* \cdot \boldsymbol{P}_j}{m_R (m_R + E_R)} \right]. \tag{A14}$$

Step 7. If $P_j^\mu d\sigma_{\mu k}$ is positive,

$$N_k^+ \to N_k^+ + \frac{P_j^\mu d\sigma_{\mu k}}{E_j^*}. \tag{A15}$$

If $P_j^\mu d\sigma_{\mu k}$ is negative,

$$N_k^- \to N_k^- + \frac{|P_j^\mu d\sigma_{\mu k}|}{E_j^*}. \tag{A16}$$

Here, N_k^+ (N_k^-) is to be proportional to the number of ρ mesons which are emitted from (absorbed by) the kth fluid element.

Step 8. If the rapidity of a negative pion Y_j which is evaluated from $\boldsymbol{p}_j$ enters in a rapidity window $Y - \Delta Y/2 < Y_j < Y + \Delta Y/2$ and $P_j^\mu d\sigma_{\mu k}$ is positive,

$$\Delta N_k^+(Y) \to \Delta N_k^+(Y) + \frac{P_j^\mu d\sigma_{\mu k}}{E_j^*}. \quad \text{(A17)}$$

If Y_j also enters the above rapidity window but $P_j^\mu d\sigma_{\mu k}$ is negative,

$$\Delta N_k^-(Y) \to \Delta N_k^-(Y) + \frac{|P_j^\mu d\sigma_{\mu k}|}{E_j^*}. \quad \text{(A18)}$$

Step 9. Repeat steps 7 and 8 for all $\tilde{N}$ random variables.

Step 10. Obtain the rapidity distribution of decay particles from the kth fluid element:

$$\frac{dN_k}{dY}(Y) = \frac{N_k^R}{N_k^+ + N_k^-}\left[\frac{\Delta N_k^+(Y) - \Delta N_k^-(Y)}{\Delta Y}\right]. \quad \text{(A19)}$$

It should be noted that the minus sign in the bracket of Eq. (A19) represents the *net* number of emitted particles from the kth fluid element, which is consistent with the Cooper-Frye prescription. For the normalization in Eq. (A19), we use the gross number $N_k^+ + N_k^-$ since this number is positive definite.

Step 11. Repeat the above steps from 1 to 10 for all fluid elements obtained in a numerical simulation of the hydrodynamic model. Summing over the contribution from all fluid elements on the freeze-out hypersurface Σ, we obtain the rapidity distribution of negative pions which are from ρ decays:

$$\frac{dN_{\rho\to\pi^- X}}{dY}(Y) = \sum_k \frac{dN_k}{dY}(Y). \quad \text{(A20)}$$

[1] S.A. Bass, Nucl. Phys. **A698**, 164 (2002); X.-N. Wang, *ibid.* **A698**, 296 (2002).
[2] P. Huovinen, Acta. Phys. Pol. B **33**, 1635 (2002).
[3] K. Adcox *et al.*, PHENIX Collaboration, Phys. Rev. Lett. **88**, 022301 (2002).
[4] R.J.M. Snellings, STAR Collaboration, Nucl. Phys. **A698**, 193 (2002).
[5] M. Gyulassy, I. Vitev, X.-N. Wang, and P. Huovinen, Phys. Lett. B **526**, 301 (2002).
[6] T. Hirano, Phys. Rev. C **65**, 011901(R) (2002).
[7] J.-Y. Ollitrault, Phys. Rev. D **46**, 229 (1992).
[8] D. Teaney and E.V. Shuryak, Phys. Rev. Lett. **83**, 4951 (1999).
[9] P.F. Kolb, J. Sollfrank, and U. Heinz, Phys. Rev. C **62**, 054909 (2000).
[10] U. Ornik, M. Plumer, B.R. Schlei, D. Strottman, and R.M. Weiner, Phys. Rev. C **54**, 1381 (1996).
[11] J. Sollfrank, P. Huovinen, M. Kataja, P.V. Ruuskanen, M. Prakash, and R. Venugopalan, Phys. Rev. C **55**, 392 (1997).
[12] C.M. Hung and E.V. Shuryak, Phys. Rev. C **57**, 1891 (1998).
[13] K. Morita, S. Muroya, H. Nakamura, and C. Nonaka, Phys. Rev. C **61**, 034904 (2000); T. Ishii and S. Muroya, Phys. Rev. D **46**, 5156 (1992).
[14] N.S. Amelin, E.F. Staubo, L.P. Csernai, V.D. Toneev, K.K. Gudima, and D. Strottman, Phys. Rev. Lett. **67**, 1523 (1991).
[15] D.H. Rischke, S. Bernard, and J.A. Maruhn, Nucl. Phys. **A595**, 346 (1995); D.H. Rischke, Y. Pürsün, and J.A. Maruhn, *ibid.* **A595**, 383 (1995).
[16] C. Nonaka, E. Honda, and S. Muroya, Eur. Phys. J. C **17**, 663 (2000).
[17] T. Hirano, K. Tsuda, and K. Kajimoto, nucl-th/0011087.
[18] T. Osada, C.E. Aguiar, Y. Hama, and T. Kodama, nucl-th/0102011.
[19] V.K. Magas, L.P. Csernai, and D. Strottman, hep-ph/0202085.
[20] J. Cleymans and H. Satz, Z. Phys. C **57**, 135 (1993).
[21] P. Braun-Munzinger, J. Stachel, J.P. Wessels, and N. Xu, Phys. Lett. B **344**, 43 (1995); **365**, 1 (1996); P. Braun-Munzinger, I. Heppe, and J. Stachel, *ibid.* **465**, 15 (1999).
[22] J. Cleymans and K. Redlich, Phys. Rev. Lett. **81**, 5284 (1998); Phys. Rev. C **60**, 054908 (1999).
[23] F. Becattini, J. Cleymans, A. Keranen, E. Suhonen, and K. Redlich, Phys. Rev. C **64**, 024901 (2001).
[24] P. Braun-Munzinger, D. Magestro, K. Redlich, and J. Stachel, Phys. Lett. B **518**, 41 (2001).
[25] M. Kaneta and N. Xu, J. Phys. G **27**, 589 (2001).
[26] E. Schnedermann, J. Sollfrank, and U. Heinz, Phys. Rev. C **48**, 2462 (1993).
[27] W. Broniowski and W. Florkowski, Phys. Rev. Lett. **87**, 272302 (2001).
[28] See, for example, E.V. Shuryak, Nucl. Phys. **A661**, 119 (1999); U. Heinz, *ibid.* **A661**, 140 (1999).
[29] For our preliminary results, see T. Hirano and K. Tsuda, in *Proceedings of the International Workshop on Gross Properties of Nuclei and Nuclear Excitation*, Hirschegg, Austria, 2002, edited by M. Buballa *et al.* (GSI, Darmstadt, 2002), p. 152.
[30] U. Ornik and R.M. Weiner, Phys. Lett. B **263**, 503 (1991).
[31] J. Sollfrank, P. Koch, and U. Heinz, Z. Phys. C **52**, 593 (1991).
[32] T. Hirano, Phys. Rev. Lett. **86**, 2754 (2001).
[33] C. Adler *et al.*, STAR Collaboration, Phys. Rev. Lett. **86**, 4778 (2001).
[34] B.B. Back *et al.*, PHOBOS Collaboration, Phys. Rev. Lett. **87**, 102301 (2001).
[35] I.G. Bearden *et al.*, PHENIX Collaboration, Phys. Rev. Lett. **87**, 112305 (2001).
[36] K. Adcox *et al.*, PHENIX Collaboration, Phys. Rev. Lett. **88**, 242301 (2002).
[37] H. Bebie, P. Gerber, J.L. Goity, and H. Leutwyler, Nucl. Phys. **B378**, 95 (1992).
[38] R. Rapp, Phys. Rev. C **66**, 017901 (2002).
[39] Particle Data Group, D.E. Groom *et al.*, Eur. Phys. J. C **15**, 1 (2000).
[40] B.B. Back *et al.*, PHOBOS Collaboration, Phys. Rev. Lett. **87**, 102303 (2001).
[41] P.F. Kolb, U. Heinz, P. Huovinen, K.J. Eskola, and K. Tuominen, Nucl. Phys. **A696**, 197 (2001).
[42] T. Hirano, K. Morita, S. Muroya, and C. Nonaka, Phys. Rev. C **65**, 061902(R) (2002); K. Morita, S. Muroya, C. Nonaka and

T. Hirano, Phys. Rev. C **66**, 054904 (2002).
[43] J. Sollfrank, P. Huovinen, and P.V. Ruuskanen, Eur. Phys. J. C **6**, 525 (1999).
[44] J.D. Bjorken, Phys. Rev. D **27**, 140 (1983).
[45] N. Arbex, F. Grassi, Y. Hama, and O. Socolowski, Phys. Rev. C **64**, 064906 (2001).
[46] F. Cooper and G. Frye, Phys. Rev. D **10**, 186 (1974).
[47] Y.M. Sinyukov, Z. Phys. C **43**, 401 (1989); K.A. Bugaev, Nucl. Phys. **A606**, 559 (1996); C. Anderlik, Z.I. Lazar, V.K. Magas, L.P. Csernai, H. Stöcker, and W. Greiner, Phys. Rev. C **59**, 388 (1999); C. Anderlik, L.P. Csernai, F. Grassi, W. Greiner, Y. Hama, T. Kodama, Z.I. Lazar, V.K. Magas, and H. Stöcker, *ibid.* **59**, 3309 (1999).
[48] C. Adler *et al.*, STAR Collaboration, Phys. Rev. Lett. **87**, 112303 (2001).
[49] M. Calderon de la Barca Sanchez, Ph.D. thesis, Yale University, 2001.
[50] K.H. Ackermann *et al.*, STAR Collaboration, Phys. Rev. Lett. **86**, 402 (2001).
[51] P.F. Kolb, P. Huovinen, U. Heinz, and H. Heiselberg, Phys. Lett. B **500**, 232 (2001).
[52] X.-N. Wang, Phys. Rev. C **63**, 054902 (2001); M. Gyulassy, I. Vitev, and X.N. Wang, Phys. Rev. Lett. **86**, 2537 (2001).
[53] I.C. Park *et al.*, PHOBOS Collaboration, Nucl. Phys. **A698**, 564 (2002); here we use updated data, B.B. Back *et al.*, PHOBOS Collaboration, nucl-ex/0205021.
[54] P.K. Sahu, N. Otuka, and A. Ohnishi, nucl-th/0206010.
[55] T. Hirano and Y. Nara, Phys. Rev. C (to be published).
[56] C. Adler *et al.*, STAR Collaboration, Phys. Rev. Lett. **87**, 182301 (2001).
[57] P. Huovinen, P.F. Kolb, U.W. Heinz, P.V. Ruuskanen, and S.A. Voloshin, Phys. Lett. B **503**, 58 (2001).
[58] D. Teaney, J. Lauret, and E.V. Shuryak, Phys. Rev. Lett. **86**, 4783 (2001); nucl-th/0110037.
[59] See, for example, G. Baym, Acta Phys. Pol. B **29**, 1839 (1998); U. Heinz and B.V. Jacak, Annu. Rev. Nucl. Part. Sci. **49**, 529 (1999).
[60] B.R. Schlei, U. Ornik, M. Plumer, and R.M. Weiner, Phys. Lett. B **293**, 275 (1992).
[61] D.H. Rischke and M. Gyulassy, Nucl. Phys. **A608**, 479 (1996).
[62] C. Adler *et al.*, STAR Collaboration, Phys. Rev. Lett. **87**, 082301 (2001).
[63] K. Adcox *et al.*, PHENIX Collaboration, Phys. Rev. Lett. **88**, 192302 (2002).
[64] S. Soff, S.A. Bass, and A. Dumitru, Phys. Rev. Lett. **86**, 3981 (2001).
[65] D. Zschiesche, S. Schramm, H. Stöcker, and W. Greiner, Phys. Rev. C **65**, 064902 (2002).
[66] U. Heinz and P.F. Kolb, Nucl. Phys. **A702**, 269 (2002).
[67] S. Soff, in *Proceedings of the International Workshop on Gross Properties of Nuclei and Nuclear Excitation* [29], p. 222.
[68] S. Bass and A. Dumitru, Phys. Rev. C **61**, 064909 (2000).
[69] See, for example, T. Hatsuda, Nucl. Phys. **A698**, 243 (2002).
[70] D. Teaney, nucl-th/0204023.